

# Dynamic analysis of soil-nailed slope

**1 Aniruddha Sengupta** PhD  
Associate Professor, Indian Institute of Technology Kharagpur,  
Kharagpur, India

**2 Debabrata Giri** PhD  
Assistant Professor, Parala Maharaja Engineering College, Orissa,  
India



An analytical method based on the kinematic limit approach is presented for stability analysis of nailed soil slopes. Earthquake effects were considered in an approximate manner in terms of seismic coefficient-dependent horizontal forces. Two kinds of failure surfaces, a planar failure surface and a circular failure surface, were considered in this study. The proposed method can be viewed as an extension of the method of slices, but it provides a more accurate treatment of forces because they are represented in an integral form. The factor of safety and nail forces obtained by the proposed method were found to be in good agreement with the published results for an 8 m high vertical soil-nailed wall.

## Notation

Basic SI units are given in parentheses.

$c$	cohesion of soil (N/m <sup>2</sup> )
$F_s$	factor of safety (dimensionless)
$G$	weight of soil wedge (N/m)
$H$	height of slope (m)
$h$	height of elementary slice (m)
$K_h$	horizontal seismic acceleration coefficient (dimensionless)
$K_t$	average tensile strength of reinforcement (N/m)
$N$	normal force on the base of slice (N/m)
$n$	number of reinforcement layers (dimensionless)
$R$	maximum shear resistance acting on the base of slice (N/m)
$S$	shear force on the base of slice (N/m)
$T_i$	tensile strength of reinforcement per unit horizontal spacing (N/m)
$T_{\max}$	maximum axial force in nail (kN)
$t$	thickness of rupture layer (mm)
$[v]$	velocity jump vector (dimensionless)
$\alpha$	angle of inclination of reinforcement (°)
$\beta$	slope angle (°)
$\gamma$	unit weight of soil (kN/m <sup>3</sup> )
$\dot{\epsilon}$	strain rate (dimensionless)
$\theta$	angle of failure plane (°)
$\lambda$	non-negative scalar multiplier (dimensionless)
$\xi$	angle of inclination of reinforcement with velocity of discontinuity (°)
$\phi$	soil friction angle (°)
$\dot{\omega}$	angular velocity of rotation (rad/s)

## 1. Introduction

Soil nailing is one of the recent techniques available for stabilising in situ soil slopes or cuts. The process of soil nailing includes installation of nails in excavated cuts or in slopes either by driving or grouting in predrilled holes. The stability of the slope face between nails is ensured by providing thin layers of shotcrete reinforced with wire mesh. The nails are generally steel bars, metal tubes or other metal rods that can resist not only tensile force but also shear stress and bending moment. The nailing method has been used in both granular and cohesive soils and in relatively heterogeneous deposits.

The general consensus among practising engineers is that soil-nailed walls perform reasonably well under seismic conditions. However, documented performance of soil-nailed systems is almost non-existent in the literature. Most of the literature (Gassler, 1988; Koseki *et al.*, 1998; Matsuo *et al.*, 1998; Sakaguchi, 1996; Sivakumar Babu and Singh, 2008) on nailed soil structures emphasises the mechanism of reinforcement and the design of structures under static load only. The failure mechanisms for slopes under static loading have typically been extended to stability analysis of slopes under seismic loading using a pseudo-static approach (Mononobe and Matsuo, 1929), but the effects of seismic excitation on the failure pattern of slopes have not been addressed. Only a handful of full-scale and model tests in the laboratory have been conducted on a soil-nailed system (Giri and Sengupta, 2009; Tufenkjian and Vucetic, 2000; Vucetic *et al.*, 1993). Consequently only limited data on the earthquake resistance and corresponding failure mechanisms for steep nailed slopes are available to date. The seismic

resistance and the failure mechanism of a nailed soil slope during an earthquake event are not clearly understood and need to be investigated properly.

There are several methods currently available for the design of soil-nailed slopes, such as the German method (Stocker *et al.*, 1979), the Davis method (Mitchell and Villet, 1987), the method developed by Gassler and Gudehus (1981), the French method (Schlosser, 1982), and the finite-element method (Dawson *et al.*, 1999, Griffiths and Lane, 1999). The first four methods are based on the limit equilibrium approach whereas the fifth one is based on the limit analysis. The finite-element method is certainly the most comprehensive approach to analyse the performance of soil structures subjected to seismic loading. However, it requires accurate measurement of the properties of the component materials, which is often difficult to achieve. In addition, further difficulties arise from modelling failure in frictional materials. The majority of the existing methods of design and analysis of a soil-nailed system are based on the pseudo-static approach, where the effect of earthquake on a potential failure soil mass is represented by a horizontal force acting at the centre of gravity. The horizontal force is calculated as the product of a seismic intensity coefficient and the weight of the potential sliding mass. The stability of soil structures under this force is expressed by a factor of safety which is usually defined as the ratio of the resisting force to the destabilising force. Failure occurs when the safety factor drops below 1. However, pseudo-static analysis is generally considered conservative, since even when the factor of safety drops below 1, the soil structures could experience a finite displacement rather than a complete failure.

An alternative analytical method is presented here based on the kinematics theorem of limit analysis to study the stability of reinforced slopes under the seismic loading condition. The kinematic theorem (Juran *et al.*, 1988, 1990) states that slopes will collapse if the rate of work done by external loads and body forces exceeds the energy dissipation rate for any assumed kinematically admissible failure mechanism. Soil deformation is assumed to be plastic and failure is associated with Coulomb's yield condition.

In the present approach, the following assumptions were made.

- (a) The effect of pore pressure build-up and change of soil strength due to earthquake shaking were ignored. In most cases, weep holes are provided in the walls for safe drainage of water from behind the wall. Furthermore, the backfill soil is usually chosen as cohesionless and free-draining material.
- (b) The slope is made of homogeneous cohesionless soil. Strictly speaking, soil is not a homogeneous material, but it is often assumed to be one, only to simplify the calculations in hand.
- (c) The reinforcement layers are finite in number and have the same length. Seldom, nails of different length and dimension are utilised in a wall construction.
- (d) The resistance to shear, bending and compression is ignored.

The nails are typically not designed for bending and compressional loads.

- (e) The critical failure surface is assumed to pass through the toe of the slopes. For the shallow failure surfaces, spalling of the face wall is ignored as they may not necessarily represent the critical case.
- (f) The available pullout resistance is assumed to be either the bond strength between soil and reinforcement or the tensile strength of the reinforcement, whichever is smaller. This is a very common assumption in the traditional design of bond length.

Under the above assumptions, the reinforcements provide tensile forces acting in the horizontal direction. The rate of external work is due to soil weight and inertia force induced by the earthquake and the only contribution to energy dissipation is that provided by the reinforcement.

The possible failure modes considered are illustrated in Figures 1 to 3.

Figure 1 shows a rotational mechanism involving a circular failure surface passing through the toe of a slope of height,  $H$ , angle,  $\beta$ , and with reinforcements of uniform length,  $L_T$ . The circular failure surface may extend within (in Figure 1(a)) and also beyond (in Figure 1(b)) the reinforced zone. Figure 2 shows a translational slope failure mechanism. Figure 3 shows the direct sliding mechanism, in which the reinforced soil mass slides over the bottom layers. Let us assume that a rigid plastic body occupies a domain  $V$  and  $v$  is a velocity field on  $V$  with a discontinuous boundary  $S$ . When a particle tends to move to  $S$  from the negative side to the positive side of the velocity field, a unit velocity vector normal to  $S$  can be defined as a velocity jump vector (Jacov, 1996). As shown in Figures 1 to 3, the velocity jump vector,  $v$ , makes an angle equal to the angle of friction  $\phi$  with the failure surface(s). The slope is unstable when one of the above-considered failure mechanisms occurs.

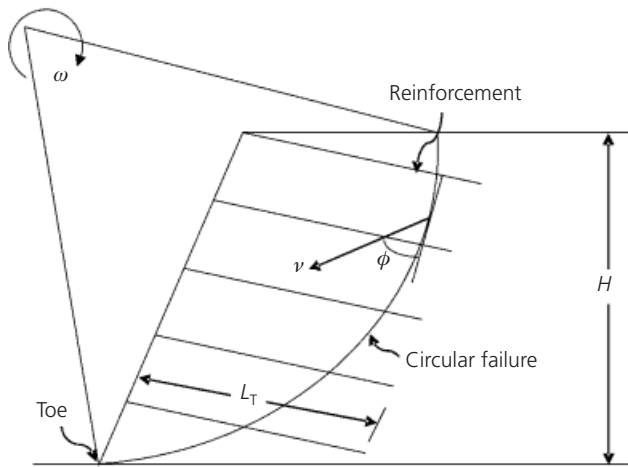
## 2. Methods of analysis

An analytical method based on the kinematics limit equilibrium (Juran *et al.*, 1988, 1990) is presented for the stability analysis of nailed soil slopes. It is assumed in kinematic approach of limit analysis that the soil and the reinforcements are perfectly plastic and their deformation is governed by associated flow rule.

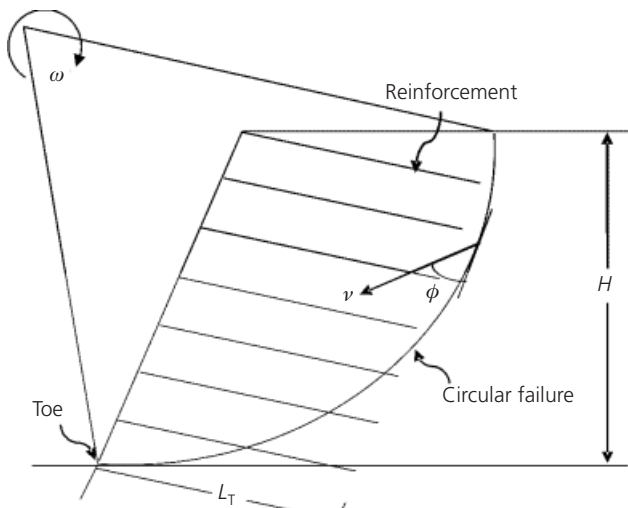
$$\text{Mathematically, } \dot{\varepsilon}_{ij}^{p1} = \lambda \frac{\partial f(\sigma_{ij})}{\partial \sigma_{ij}}$$

1.  $\lambda \geq 0$  if  $f = 0$  and  $\lambda = 0$  if  $f < 0$

Where  $\dot{\varepsilon}_{ij}^{p1}$  is the plastic strain rate tensor in a kinematically admissible velocity field,  $\sigma_{ij}$  is the stress tensor associated with strain rate tensor,  $\lambda$  is a non-negative scalar multiplier and  $f(\sigma_{ij}) = 0$  is the yield criteria. Mohr–Coulomb failure criteria



(a)



(b)

Figure 1. Circular failure surface: (a) extended within reinforced zone; (b) extended beyond reinforced zone

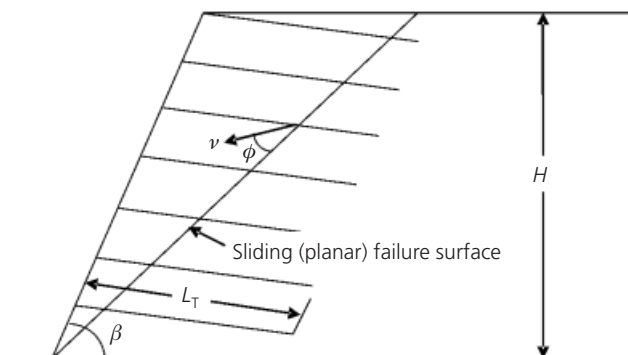


Figure 2. Translational slope failure mechanism

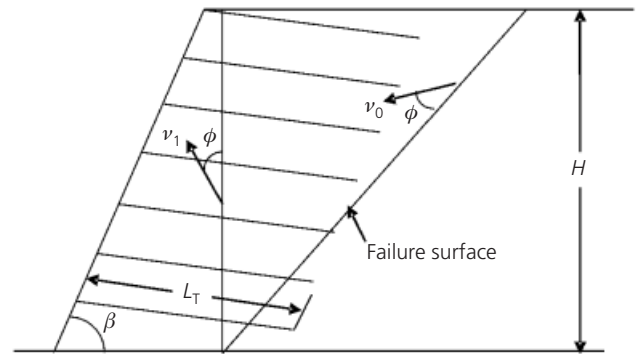


Figure 3. Direct sliding mechanism

are assumed and the discontinuity vector (velocity jump) is assumed to be inclined to the rupture surface at the angle of internal friction,  $\phi$ .

The kinematics theorem of limit analysis (Juran *et al.*, 1988, 1990) states that when the rate of work done by the external forces and the body forces exceeds the rate of internal dissipation energy, the structure will collapse. This theorem is usually referred to as the upper bound theorem, because it allows the calculation of an upper bound to the limiting force causing failure.

Michalowski (1998) represented this theorem mathematically as

$$2. \int_V D(\dot{\epsilon}_{IJ})dV \geq \int_S T_i v_i dS + \int_V \gamma_i v_i dV$$

The left-hand side of the equation represents the rate of energy dissipation ( $D$ ) during an incipient failure of a structure and the right-hand side includes the rate of work done by all the external forces. In the above equation,  $T_i$  is the stress vector on the boundary  $S$ ,  $v_i$  is the velocity vector in the kinematically admissible mechanism.  $\gamma_i$  is the specific weight and  $V$  is the volume of the mechanism (refer to Figure 4). The mathematical form of the theorem states that the rate of energy dissipation is not less than the rate of work done by external forces in any kinematically admissible failure mechanism. The total force on the boundary,  $S$ , can be calculated only if velocity,  $v_i$ , on this boundary is constant. If the geometry of the structure is given and all loads and material parameters are known, the safety factor can be calculated. Earthquake effects are considered in terms of seismic coefficient-dependent horizontal forces. Two kinds of failure surfaces were considered in this study, namely a planar failure surface and a circular failure surface. The proposed method is an extension of the method of slices (Duncan and Wright, 2005), but it provides a more accurate treatment of forces because they are represented in an integral form.





and opposite and parallel to the base of slice of.  $\sum(X_1 - X_T)$  is zero for the whole failure mass.

Resolving the forces acting on the base of slice of

$$13. \quad dN = \gamma h dx \cos \theta - K_h \gamma h dx \sin \theta$$


---

$$14. \quad dS = \gamma h dx \sin \theta + K_h \gamma h dx \cos \theta$$


---

$$15. \quad \text{where } \theta = \sin^{-1} (x - a)/r \text{ and } r = \sqrt{a^2 + b^2}$$


---

The force  $dN$  can produce a maximum shearing resistance  $dR$  given by

$$dR = c dx \sec \theta + \gamma h dx (\cos \theta - \sin \theta) \tan \phi$$

$$16. \quad dR = c dx \sec \theta + \gamma h dx (\cos \theta - \sin \theta) \tan \phi$$


---

where  $c$  is the cohesion of the soil.

The equation of line, AB, in Figure 6, is

$$17a. \quad y_1 = x \tan \beta$$


---

The equation of line BC is

$$17b. \quad y_2 = H$$


---

The equation of the circular failure surface AC is

$$17c. \quad y_3 = b - \sqrt{r^2 - (x - a)^2}$$


---

Then the total rate of work done can be equal to the sum of work done by  $dS$  and is given by

$$\dot{W} = \gamma v \cos \phi \left\{ \sin \theta \left[ \int_0^l (y_1 - y_3) dx + \int_l^L (H - y_3) dx \right] + K_h \cos \theta \left[ \int_0^l (y_1 - y_3) dx + \int_l^L (H - y_3) dx \right] \right\}$$

$$18. \quad = \gamma v \cos \phi (I_s + K_h I_c)$$


---

where

$$I_s = \int_0^l (y_1 - y_3) (\sin \theta dx) + \int_l^L (y_2 - y_3) \sin \theta dx$$

$$19. \quad = (H^2/2) [(a \cot \beta + b) - (H/3) \operatorname{cosec}^2 \beta]$$


---

$$I_c = \int_0^l (y_1 - y_3) \cos \theta dx + \int_l^L (y_1 - y_3) \cos \theta dx$$

$$= \frac{\tan \beta}{6r} [2r^2 + (l - a)^2] \sqrt{r^2 - (l - a)^2} + \frac{b \tan \beta}{r} \left( \frac{a^2}{2} + \frac{b^2}{3} \right) + \frac{r}{2} (a \tan \beta - H) \sin^{-1} \left( \frac{l - a}{r} \right) + \frac{r}{2} (a \tan \beta - b) \sin^{-1} \frac{a}{r} - \frac{r}{2} (b - H) \sin^{-1} \left( \frac{L - a}{r} \right)$$

$$20. \quad + \frac{1}{6r} [4r^2 L - ab^2 + (L - a)(H - a)^2]$$


---

where

$$l = H \cot \beta \text{ and}$$

$$21. \quad L = a + \sqrt{r^2 - (b - H)^2} \quad l = H \cot \beta$$


---

The rate of dissipation of internal energy is due to shear resistance and is given by

$$\begin{aligned} \dot{D} &= \int dR v \cos \phi \\ &= v \cos \phi \left[ \int_0^L c \sec \theta dx + \int_0^l \gamma (y_1 - y_3) (\cos \theta - K_h \sin \theta) \tan \phi dx + \int_l^L \gamma (y_2 - y_3) (\cos \theta - K_h \sin \theta \tan \phi) dx \right] \end{aligned}$$

$$22. \quad = v \cos \phi [rc\phi + \gamma \tan \phi (I_c - K_h I_s)]$$


---

where

$$23. \quad \phi = \sin^{-1} [(L - a)/r] + \sin^{-1} (a/r)$$


---

The rotational failure mechanism is represented by a circular

failure surface. For a given slope angle and internal angle of friction, the toe failure is fully described by two parameters  $\vartheta_0$  and  $\vartheta_f$  as shown in Figure 6. Rupture of the reinforcement is interpreted as a plastic flow process consistent with the flow rule. The energy dissipation rate in a single reinforcement intersecting a velocity discontinuity can be derived assuming that the discontinuity is of finite-thickness,  $t$ , with a high-velocity gradient as shown in Figure 7.

The reinforcement contributes to the stability of the structures only through its tensile strength (reinforcement resistance to shear, torsion and bending is neglected). The kinematics requires that the velocity jump vector  $[v]$  be inclined to the velocity discontinuity at an angle of internal friction  $\phi$ . The reinforcement is inclined to the velocity discontinuity at an angle  $\xi$  as shown in Figure 7. No reinforcement is assumed to be pulled out and sector PQ with length  $(t/\sin \xi)$  (where  $t$  is the thickness of rupture layer) is subjected to plastic flow. The rate of energy dissipation in a single reinforcement intersecting a velocity discontinuity per unit horizontal spacing of reinforcement may be calculated as

$$D = \int_0^{(t/\sin \xi)} T_1 \dot{\epsilon} dx$$

$$24. \quad = T_1 [v] \cos(\xi - \phi)$$

where  $T_1$  is the limit tensile force in the reinforcement per unit horizontal spacing and  $\dot{\epsilon}$  is the strain rate in the direction of reinforcement.

The strain rate in the reinforcement is given by

$$25. \quad \dot{\epsilon} = [v] \frac{\cos(\xi - \phi)}{t \sin \xi}$$

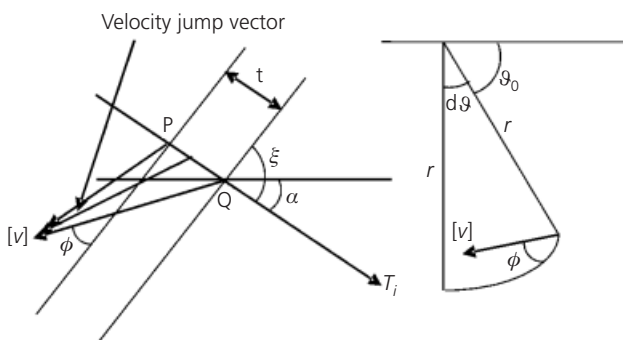


Figure 7. Velocity jump vector

The average strength  $K_t$  of reinforcement is given by

$$26. \quad K_t = n T_1 \frac{\cos \alpha}{H}$$

where  $n$  is the number of reinforcement layers.

The energy dissipation rate per unit area of the discontinuity surface becomes

$$\dot{D} = \int_0^{t/\sin \xi} K_t \sin \xi dx \dot{\epsilon}$$

$$27. \quad = K_t [v] \cos(\xi - \phi) \sin \xi$$

For a circular failure surface, the energy dissipation rate per infinitesimal length ( $r d\vartheta$ ) increment (refer to Figure 7) is given by

$$28. \quad d\dot{D} = K_t \dot{\omega} r^2 \int \cos(\vartheta + \alpha - \phi) \sin(\vartheta + \alpha) d\vartheta$$

where  $\dot{\omega}$  is the rate of rotation.

Integrating from  $\vartheta_0$  to  $\vartheta_f$  and assuming  $K_t$  to be constant

$$\dot{D} = K_t \dot{\omega} r^2 \int_{\vartheta_0}^{\vartheta_f} \cos(\vartheta + \alpha - \phi) \sin(\vartheta + \alpha) d\vartheta$$

$$= K_t \dot{\omega} r^2 \{ \cos \phi \{ [\sin^2(\vartheta_0 + \alpha) - \sin^2(\vartheta_f + \alpha)] / 2 \}$$

$$+ \sin \phi \{ [(\vartheta_f - \vartheta_0) / 2]$$

$$- [(\sin 2(\vartheta_f + \alpha)) / 4]$$

$$+ [(\sin 2(\vartheta_0 + \alpha)) / 4] \}$$

$$29. \quad + [(\sin 2(\vartheta_0 + \alpha)) / 4] \}$$

The total rate of internal energy dissipation is the sum of cohesive and tensile reinforcement forces and is given by

$$\dot{D} = v \cos \phi [rc \phi + \gamma \tan \phi (I_c - K_h I_s)]$$

$$+ K_t \dot{\omega} r^2 \{ \cos \phi \{ [\sin^2(\vartheta_0 + \alpha) - \sin^2(\vartheta_f + \alpha)] / 2 \}$$

$$+ \sin \phi \{ [(\vartheta_f - \vartheta_0) / 2]$$

$$- [(\sin 2(\vartheta_f + \alpha)) / 4]$$

$$30. \quad + [(\sin 2(\vartheta_0 + \alpha)) / 4] \}$$

The factor of safety,  $F_s$ , is calculated by taking the ratio of Equations 30 and 18, and is given by

$$F_s = \frac{rc\psi + \gamma \tan \phi (I_c - K_h I_s)}{\gamma (I_s + K_h I_c)} + K_t r \left( \frac{\{[\sin^2(\vartheta_0 + \alpha) - \sin^2(\vartheta_f + \alpha)]/2\}}{\gamma (I_s + K_h I_c)} + \tan \phi \left\{ \frac{[(\vartheta_f - \vartheta_0)/2] - [(\sin 2(\vartheta_f + \alpha))/4]}{+[(\sin 2(\vartheta_0 + \alpha))/4]} \right\} \right) \quad (31)$$

It may be observed from Equation 31 that the factor of safety for a given slope is a function of parameters such as the coordinate of failure circle ( $a$ ,  $b$ ), angle  $\vartheta_f$  and  $\vartheta_0$ , and angle  $\alpha$ . Thus minimum value of  $F_s$  can be found using the minimisation technique.

### 3. Verification of the proposed method

The published results reported by Sivakumar Babu and Singh (2008) for a soil-nailed wall supporting a vertical cut of 8 m high under seismic condition were utilised here to verify the present method of analysis. The geometry of the soil-nailed wall supporting the vertical cut is shown in Figure 8. The 8 m high wall was designed in conventional manner by using the allowable stress design procedure. The soil nails were 4.7 m long and placed in 100 mm diameter drill holes. They were grouted in place at 1 m apart at an angle of 15° with the horizontal axis. The wall was analysed numerically by using the finite-element method. The seismic records from Bhuj (Iyengar and Raghu Kanth, 2002) and Uttarkashi (Chandrasekaran and Das, 1992) earthquakes were utilised in the reported pseudo-static and dynamic analyses of the wall. The external failure mode of the nailed soil wall in terms of global stability and sliding stability was studied under static, pseudo-static as well as dynamic conditions. In the present study, the published pseudo-static results reported in the paper were compared with the results of the present analysis. The horizontal seismic coefficient,  $k_h$ , for the pseudo-static analysis corresponding to the Bhuj and Uttarkashi earthquake was adopted from the paper and given as 0.106 and 0.241, respectively. All other material parameters adopted from the literature (Sivakumar Babu and Singh 2008) and utilised in the present analysis are given in

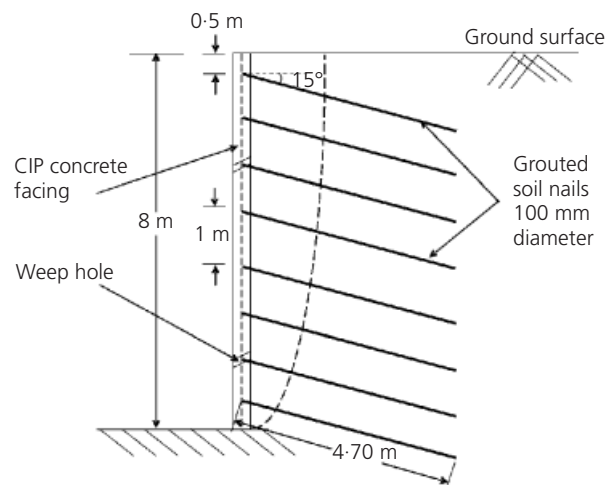


Figure 8. The geometry of the soil-nailed wall supporting an 8 m vertical cut

Table 1. Since the critical failure surface in the backfill was not given in the referred paper, it was found by the minimisation technique and shown in Figure 8. The factor of safety corresponding to the failure surface was first calculated from Equation 31. The total rate of internal energy dissipated was reduced from the corresponding factor of safety value. The rate of internal energy dissipated due to tensile reinforcement force was obtained from the value of total energy dissipated. The tensile force in the reinforcements was calculated from Equation 26. In the above calculations, the velocity jump vector  $[v]$  was kept constant, as factor of safety value is independent of velocity jump. Table 2 shows the comparison between the published results and the results from the present theory. The factors of safety against global stability of the nailed wall for the Bhuj and Uttarkashi earthquakes were found to be 0.91 and 0.78, respectively. These values are comparable with the corresponding published results (0.95 and 0.81). The maximum axial force in the nails as predicted by the present method was found to be 32.4 and 37.98 kN, respectively, for the Bhuj and Uttarkashi earthquakes. These values are also comparable with the corresponding published results.

Parameter	Value
Cohesion of the backfill soil, $c$ : kPa	1.0
Friction angle of the backfill soil, $\phi$ : °	30.0
Unit weight of the backfill soil, $\gamma$ : kN/m <sup>3</sup>	16.0
Slope angle, $\beta$ : °	0.0
Angle of inclination of nails, $\alpha$ : °	15.0
Nail length: m	4.7
Maximum axial tensile load capacity of nails, $T_i$ : kN	83.44

Table 1. Material parameters for the soil-nailed wall

Parameters	Published results from Sivakumar Babu and Singh (2008)		Results from the present method of analysis	
	For Bhuj equation	For Uttarkashi equation	For Bhuj equation	For Uttarkashi equation
Maximum axial force in nail, $T_{max}$ , (kN)	34.5	40.73	32.4	37.98
Factor of safety against global stability	0.95	0.81	0.91	0.78

**Table 2.** Comparison of present method of analysis with published results for an 8 m high vertical soil nailed wall

#### 4. Conclusions

An analytical method based on the kinematic limit approach has been developed for stability analysis of soil-nailed slopes. Two kinds of failure surfaces, a planar and a circular failure surface, are considered in the formulation. The proposed method can be viewed as an extension of the method of slices, but it provides a more accurate treatment of forces because they are represented in an integral form. The published result of a soil nail wall supporting a vertical cut of 8 m high is utilised to verify the performance of the new methodology. The maximum axial force in the nails and the factor of safety predicted by the proposed method are found to be in good agreement with the corresponding published results for the 8 m high soil-nailed vertical cut under seismic conditions.

#### REFERENCES

- Chandrasekaran AR and Das JD (1992) Analysis of strong ground motion accelerograms of Uttarkashi earthquake of October 20, 1991. *Bull Indian Soc Earthquake Tech* **29(1)**: 35–55.
- Dawson EM, Roth WH and Drescher A (1999) Slope stability analysis by strength reduction. *Géotechnique* **49(6)**: 835–840.
- Duncan JM and Wright SG (2005) *Soil Strength and Slope Stability*. Wiley, New York.
- Gassler G (1988) Soil nailing – theoretical basis and practical design. *Proceedings of the Geotechnical Symposium on Theory and Practice of Earth Reinforcement, Japan*. AA Balkema, Rotterdam, the Netherlands, pp. 283–288.
- Gassler G and Gudehus G (1981) Soil nailing – some aspects of a new technique. *Proceedings of the 10th International Conference on Soil Mechanics and Foundation Engineering (ICSMFE), Stockholm*, Vol 3, 665–670.
- Giri D and Sengupta A (2009) Dynamic behavior of small scale nailed soil slopes. *International Journal of Geotechnical and Geological Engineering* **27(6)**: 687–698.
- Griffiths DV and Lane PA (1999) Slope stability analysis by finite elements. *Géotechnique* **49(3)**: 387–403.
- Iyengar RN and Raghu Kanth STG (2002) Strong ground motion at Bhuj city during the Kutch earthquake. *Current Science* **82(11)**: 1366–1372.
- Jacov AK (1996) *Limit Analysis of Solids and Structures*. CRC Press, Taylor and Francis Group, New York.
- Juran I, George B, Khalid F and Elias V (1988) Kinematical limit analysis approach for the design of nailed soil retaining structures. *Proceedings of the Geotechnical Symposium on Theory and Practice of Earth Reinforcement, Japan*. AA Balkema, Rotterdam, the Netherlands, pp. 301–306.
- Juran I, George B, Khalid F and Elias V (1990) Kinematical limit analysis approach for the design of soil nailed structures. *Journal of Geotechnical Engineering, ASCE* **116(1)**: 54–71.
- Koseki J, Munaf Y, Tatsuoka F, Tateyama M, Kojima K and Sato T (1998) Shaking and tilt table tests of geosynthetic reinforced soil and conventional type retaining walls. *Geosynthetic International* **5(1–2)**: 73–96.
- Matsuo O, Tsutsumi T, Yokoyama K and Saito Y (1998) Shaking table tests and analyses of geosynthetic-reinforced soil retaining walls. *Geosynthetic International* **5(1–2)**: 97–126.
- Michalowski RL (1998) Soil reinforcement for seismic design of geotechnical structures. *Computers and Geotechnics* **23**: 1–17.
- Mitchell JK and Villet WCB (1987) *Reinforcement of Earth Slopes and Embankment*. National Cooperative Highway Research Program Transportation Research Board, New York, Report, p. 290.
- Mononobe N and Matsuo M (1929) On the determination of earth pressures during earthquakes. *Proceedings of the World Engineering Conference, Tokyo, Japan*. International Association for Earthquake Engineering, Japan, Vol. 9, pp. 177–185.
- Sakaguchi M (1996) A study of the seismic behavior of geosynthetic-reinforced walls in Japan. *Geosynthetic International* **3(1)**: 13–30.
- Schlosser F (1982) Behavior and design of soil nailing. *Proceedings of a Symposium on Recent Developments in Ground Improvement Techniques, Asian Institute of Technology, Bangkok*. pp. 399–413.
- Sivakumar Babu GL and Singh VP (2008) Numerical analysis of

---

performance of soil nail walls in seismic condition. *ISET Journal of Earthquake Technology* **45(1–2)**: 31–40.

Stocker ME, Korcber GW, Gassler G and Gudehus G (1979) Soil nailing. *Proceedings of International Conference on Soil Reinforcement*, Paris, pp. 469–474.

Tufenkjian MR and Vucetic M (2000) Dynamic failure

mechanism of soil-nailed excavation models in centrifuge. *Journal of Geotechnical and Geo-environmental Engineering* **126(3)**: 227–235.

Vucetic M, Tufenkjian MR and Doroudian M (1993) Dynamic centrifuge testing of soil-nailed excavations. *Geotechnical Testing Journal, GTJODJ* **16(2)**: 172–187.

---

**WHAT DO YOU THINK?**

To discuss this paper, please email up to 500 words to the editor at [journals@ice.org.uk](mailto:journals@ice.org.uk). Your contribution will be forwarded to the author(s) for a reply and, if considered appropriate by the editorial panel, will be published as a discussion in a future issue of the journal.

*Proceedings* journals rely entirely on contributions sent in by civil engineering professionals, academics and students. Papers should be 2000–5000 words long (briefing papers should be 1000–2000 words long), with adequate illustrations and references. You can submit your paper online via [www.icevirtuallibrary.com/content/journals](http://www.icevirtuallibrary.com/content/journals), where you will also find detailed author guidelines.